# Influence of Nickel on Biomass Pyro-Gasification: Coupled Thermodynamic and Experimental Investigations

Marwa Said, Laurent Cassayre, Jean-Louis Dirion, Ange Nzihou, Xavier Joulia

# Influence of Nickel on Biomass Pyro-Gasification: Coupled Thermodynamic and Experimental Investigations

Marwa Said,[†,‡] Laurent Cassayre,[*,†,‡] Jean-Louis Dirion,[†] Ange Nzihou,[†] and Xavier Joulia[‡]

[†]Université de Toulouse, Mines Albi, CNRS, Centre RAPSODEE, Campus Jarlard, F-81013 Albi Cedex 09, France
[‡]Laboratoire de Génie Chimique, Université de Toulouse, CNRS, Toulouse, France

**ABSTRACT:** The present research falls within the scope of the chemical influence of heavy metals on thermochemical conversion of biomass. Specifically, the impact of nickel during pyrolysis and $CO_2$-gasification of willow samples was studied by experimental and thermodynamic approaches. For this purpose, willow wood samples were impregnated with various contents of nickel. The pyro-gasification tests were performed in a laboratory fixed bed reactor, providing the chemical composition of solid residue and major gases. Our thermodynamic simulations, based on a specific calculation procedure, were found to corroborate most of the experimental data. In addition to these methodological findings, the main results of the study are (i) Ni has a noticeable catalytic activity even at low contents (between 0.016 and 0.086 mol per kg of wood), (ii) due to the low oxygen potential of the system C + $CO_2$, Ni stays in an active metal form as long as some carbon is left in the reactor, and (iii) Ni prevents the volatilization of sulfur during the gasification, due to the formation of a stable $Ni_3S_2$ solid phase.

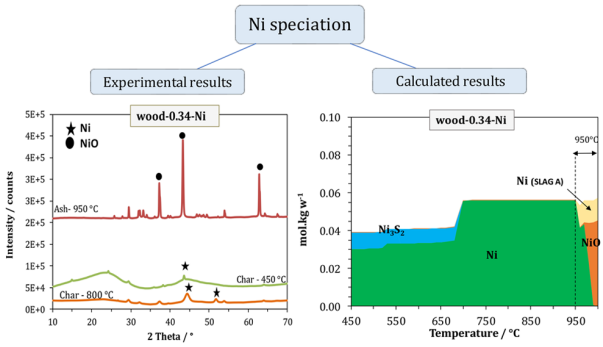


## 1. INTRODUCTION

Biomass is considered to be the only natural and renewable carbon resource that can effectively substitute fossil fuels. Additionally, it is especially abundant and stands as the third energy resource after oil and coal.[1] Among the many options for biomass processing, several thermochemical conversion processes are appealing, such as combustion for heat and electricity production, and pyro-gasification with the addition of a gasification agent such as $H_2O$ or $CO_2$. Moreover, biomass gasification in the presence of $CO_2$ would offer a potential solution for the alleviation of greenhouse gas emission.

Wastes, such as contaminated biomass, constitute widely available resources for these conversion processes. Plants used for phytoextraction represent an accessible resource of such contaminated biomass. These plants are used to extract contaminants from polluted soils, and heavy metals (HM) accumulate inside the roots, stems and leaves.[2] For example, the concentration of zinc in crops grown on contaminated soils can reach 4 g·kg$^{-1}$ in contaminated willow leaves,[3] and up to 10 g·kg$^{-1}$ of nickel in the tissues of some hyperaccumulators.[4] Houzelot et al.[5] even studied specific plants allowing nickel content as high as 150 g·kg$^{-1}$. Waste biomass such as demolition wood, chromated copper arsenate timber, deinking sludge, sewage sludge, or spent pot liner constitute many other examples of contaminated biomass that can contain high amounts of HM.

Currently, contaminated biomass is hardly used in thermochemical conversion processes, due to its potentially high content in HM. Given the large quantities of these resources, many studies investigate the behavior and the effect of the HM during their thermochemical conversion. It has been shown that HM distribute unevenly between ash, gases and tars. Their behavior mainly depends on their initial content in the biomass, and on their chemical form during the thermal conversion.[2,3] The HM vaporization, and more generally the inorganic elements behavior, has been widely studied with the aim of not only reducing the emissions of toxic elements in the environment during industrial combustion processes[6,7] but also managing related technical issues (agglomeration of fluidized beds, slag formation, deposition and corrosion phenomena on heat exchangers).[8,9]

A body of work has also shown that some HM have a significant influence on reaction kinetics. Depending on their nature, these HM have a catalytic or inhibitory effect on thermochemical conversion reactions.[10] As a consequence, finely divided particles of nickel, cobalt or iron[11] are sometimes used as catalysts in thermochemical conversion processes.

To improve the understanding of HM behavior and/or influence during thermochemical conversion of biomass, two main methods (sometimes combined) are usually applied. The first method consists of carrying out measurements and analysis of pyro-gasification products in laboratory or industrial installations. The TGAs (thermogravimetric analyzers) are usually used to identify the kinetics of the gasification reaction.[12,13] The fixed-bed reactor is widely used thanks to its ease of operation. Other studies are carried out in fluidized bed reactors, which is a widely developed industrial gasification technology.[14] For example, Šyc et al.[14] studied the behavior of Cd, Cu, Ni, Pb, and Zn during steam gasification of a mixture of oak and beech wood in a fluidized bed reactor. They showed that cadmium is the most volatile metal and that it is mainly present in the gas phase, whereas nickel is found in the ashes. The authors concluded that the vaporization of the heavy metals decreases as follows: Cd ≫ Pb > Zn > Cu > Ni. Collard et al.,[15] Bru et al.,[16] and Richardson et al.[17] inserted intentionally by impregnation, some HM (Ni, Cu, and Fe) into the biomass to improve the contact between the catalyst and the biomass and optimize the conversion efficiency. Other researchers[18,19] investigated the reactivity of various biomass chars, in the presence of different metals, in $CO_2$ atmosphere using different kinetic models to fit with the reactivity data. They found that the gasification reactivity of metal-containing chars was higher than that of the chars obtained from raw biomass.

The second approach relies on the investigation of thermodynamic calculations, which may be a valuable computational approach to predict and understand the behavior of elements during thermal treatment of biomass and waste. In some recent studies,[20−23] specific calculations procedure were developed, to take into account the highly nonequilibrium behavior of organic matter during thermal treatment and its influence on inorganics' behavior.

In the present research, we focus on understanding the impact of the nickel content on the thermal decomposition of a biomass heated in a $CO_2$ atmosphere. The methodology combines experimental measurements (in a thermogravimetric device and a fixed bed reactor) and thermodynamic simulations. The main research questions concern (i) the determination of the chemical form of nickel during the main steps of the thermal treatment (pyrolysis up to 450 °C, gasification up to 950 °C), (ii) the influence of nickel on the main conversion reactions, and (iii) on the behavior of other inorganic elements.

The selected biomass is willow, which exhibits high HM absorption capacity. Because natural contaminated biomass is very heterogeneous and usually contains many metals whose roles can interfere,[24] the willow samples were prepared by impregnation of various Ni contents. On the basis of our previous study,[25] we chose impregnation conditions adapted to the understanding of the effect of Ni without modifying the wood structure.

In the following sections, our experimental data are discussed in the light of a thermodynamic approach that we developed in previous research (databases aspects,[26] calculation procedure aspects[27]).

## 2. MATERIALS AND METHODS

**2.1. Experimental Procedure.** *2.1.1. Samples Preparation.* The willow wood pellets, supplied by "pépinières-Naudet" company (France), were dried, crushed, and sieved to a range of particle size of 0.5−1 mm. About 30 g of willow wood particles were then impregnated in 300 mL of nickel nitrate aqueous solutions, prepared with three different amounts of $Ni(NO_3)_2{\cdot}6H_2O$ (Sigma-Aldrich, 99% purity). The obtained mixtures were stirred at ambient temperature for 24 h.

According to our previous study,[25] the Ni concentration in the aqueous solution had to be below 0.1 mass %, to avoid significant modifications of the wood structure and noticeable washing of some elements (mostly Ca, K, and S). Therefore, the selected solution concentrations were 0.01, 0.05, and 0.07 mass % of Ni, respectively. The resulting Ni concentration in the impregnated wood samples were measured by elemental analysis (see section 2.1.3) and correspond to 0.09, 0.34, and 0.48 wt %, respectively. The Ni concentrations are close to those found in the literature for phytoextraction plants, where the Ni contents are usually between 0.1 and 1 wt %.[28,29]

In the following, the samples are labeled "wood-*X*-Ni", *X* being the Ni concentration (in wt %) in the wood samples. "Raw-wood" corresponds to a nonimpregnated wood.

*2.1.2. Pyro-Gasification Devices.* Thermal treatments were carried out using two devices: a fixed-bed reactor, with 5 g of wood, and a thermo-gravimetric analyzer (TGA), with 15 mg of wood.

The reactor is composed of a quartz tube, in which the wood samples are held by a sintered porous quartz disk (see our previous work[25] for more details). The wood samples are first heated at 5 °C·min$^{-1}$, under $N_2$ flow (6 L·h$^{-1}$), up to 450 °C. After 1 h at 450 °C, a mixed atmosphere (5.4 L.h$^{-1}$ of $CO_2$ and 0.6 L·h$^{-1}$ of $N_2$) is flushed in the reactor, and the furnace is heated at 5 °C·min$^{-1}$, from 450 to 950 °C. The sample is then kept for 1 h at 950 °C, before cooling. An additional experiment was carried out with wood-0.34-Ni and stopped when the temperature reached 800 °C. These operating conditions were selected to complete the sample pyrolysis before the start of the gasification. Even if there is some interference between the thermal degradation step and the gasification step, this protocol is the best compromise to illustrate the influence of Ni content on both types of reactions, and for the two reactors.

Solid residues are collected after treatment at 450 °C (henceforth char) and at 950 °C (henceforth ash). All solid samples are weighed and characterized.

The gases are collected in successive 0.5 L sampling bags and analyzed by a gas chromatograph equipped with two analytical columns. This protocol provides the quantitative amount of major gases $N_2$, $O_2$, $H_2$, CO, $CH_4$, $CO_2$, $C_2H_4$, and $C_2H_6$.

The thermogravimetric measurements are carried using a TGA/DTA analyzer (SDT Q600) under atmospheric pressure. About 15 mg of sample is placed in a platinum crucible. The analyses are performed in the same conditions (temperature and atmosphere) as in the pyro-gasification reactor. Each TGA is repeated three times, and the mean standard deviation of weight loss is lower than 1%. Due to the low initial amount of wood, the solid residues are not characterized.

*2.1.3. Sample Analyses.* The CHN contents of the different samples (raw wood, impregnated wood, char, and ash) are determined with an elemental analyzer (Flash 2000). The ash content of each sample is measured according to the standard FN-EN-ISO-18122, which consists of an air oxidation at 550 °C. The oxygen content is determined by mass balance.

For the determination of inorganics, the samples are mineralized with a specific mineralization protocol and analyzed on inductively coupled plasma optical emission spectroscopy

**Table 1. Elemental Composition of Wood Samples**

| element | mol·kgw$^{-1}$ | element | mol·kgw$^{-1}$ | element | mol·kgw$^{-1}$ |
|---|---|---|---|---|---|
| H | $59.70 \pm 3.1 \times 10^{-1}$ | P | $1.22 \times 10^{-2} \pm 1.4 \times 10^{-3}$ | Sn | $3.32 \times 10^{-4} \pm 1.7 \times 10^{-5}$ |
| C | $41.23 \pm 1.3 \times 10^{-1}$ | Mg | $7.92 \times 10^{-3} \pm 2.0 \times 10^{-3}$ | Mn | $2.66 \times 10^{-4} \pm 3.9 \times 10^{-5}$ |
| O | $27.67 \pm 1.1 \times 10^{-1}$ | Na | $6.03 \times 10^{-3} \pm 9.3 \times 10^{-4}$ | Pb | $2.25 \times 10^{-4} \pm 2.7 \times 10^{-5}$ |
| N | $0.51 \pm 5.0 \times 10^{-2}$ | Al | $2.97 \times 10^{-3} \pm 4.3 \times 10^{-4}$ | Sb | $1.81 \times 10^{-4} \pm 6.3 \times 10^{-5}$ |
| Ca | $1.03 \times 10^{-1} \pm 1.9 \times 10^{-3}$ | Cl | $2.36 \times 10^{-3} \pm 1.2 \times 10^{-3}$ | Cd | $1.65 \times 10^{-4} \pm 1.1 \times 10^{-5}$ |
| F | $7.18 \times 10^{-2} \pm 3.4 \times 10^{-2}$ | Fe | $1.45 \times 10^{-3} \pm 2.7 \times 10^{-4}$ | Cr | $1.36 \times 10^{-4} \pm 2.0 \times 10^{-5}$ |
| K | $1.96 \times 10^{-2} \pm 1.4 \times 10^{-3}$ | Zn | $7.56 \times 10^{-4} \pm 1.5 \times 10^{-4}$ | Co | $6.93 \times 10^{-5} \pm 6.3 \times 10^{-6}$ |
| S | $1.84 \times 10^{-2} \pm 2.7 \times 10^{-3}$ | B | $4.54 \times 10^{-4} \pm 9.0 \times 10^{-5}$ | Ba | $3.49 \times 10^{-5} \pm 5.7 \times 10^{-6}$ |
| Si | $1.25\times \times 10^{-2} \pm 2.6 \times 10^{-3}$ | Cu | $4.38 \times 10^{-4} \pm 7.4 \times 10^{-5}$ | | |

| Ni (mol·kgw$^{-1}$) | | | |
|---|---|---|---|
| raw wood | wood-0.09-Ni | wood-0.34-Ni | wood-0.48-Ni |
| $4.44 \times 10^{-4}$ | $1.61 \times 10^{-2}$ | $5.74 \times 10^{-2}$ | $8.45 \times 10^{-2}$ |

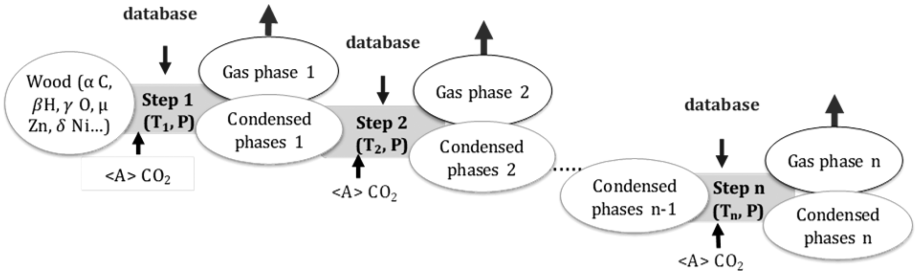


**Figure 1.** Principle of open system equilibrium calculations.

(ICP-OES). For wood and char, 200 mg samples are immersed in 2 mL of oxygenated water and 8 mL of nitric acid. The mixture is placed in a special fluoroplastic flask (PTFE), which is inserted in a pressure digestion vessel made of high alloy stainless steel SS 316 Ti (DAB-2). The vessel is heated in an electric heating block for 4 h at 200 °C under high pressure (max 200 bar). For ashes, 40 mg samples are attacked by a mixture of hydrogen peroxide and nitric acid and then heated for 10 h at 200 °C under the same conditions as those described for char. Each measurement is repeated three times.

The samples compositions are provided in Table 1, in mol per kg of wood (mol·kgw$^{-1}$). For all elements (except Ni), the reported composition is the mean value measured in the four wood samples (Raw wood, Wood-*X*-Ni with $X = 0.09$, 0.34 and 0.48). The precision indicated in Table 1 corresponds thus to the standard deviation of twelve measurements (three analyses of each four samples).

All solid residues are also characterized by X-ray diffraction, with a Philips PANalytical X'Pert MPD diffractometer using Cu ($K\alpha$) radiation. Data acquisition is performed between 10 and 70° in $2\theta$ with a step of 0.017° ($2\theta$).

**2.2. Thermodynamic Calculation Methodology.** In our previous work,[27] a specific calculation methodology was selected out of several options by comparing equilibrium calculations with the elemental composition (27 elements listed in Table 1) of raw willow wood ashes after $CO_2$ pyro-gasification. The main features of the selected procedure are presented in this section.

*2.2.1. Software and Database.* Equilibrium calculations are performed with FactSage 7.0.[30] To describe the complex system composed of 27 elements, a specific selection of the compounds available within the FactSage package led to the final choice of 373 gaseous, 247 liquid, and 1115 solid species. Within this selection, there are 10 gaseous, 10 liquid, and 66 solid Ni-containing compounds. Two liquid solution phases were also selected: (i) SALTF, which describes liquid salts solutions (Na, K//F, Cl, $CO_3$) with low melting points, and (ii) SLAGA, which describes liquid silicates solutions (Si, K, Ca// O, S) with high melting points.[31]

*2.2.2. Calculations Conditions.* The calculations are performed on 1 kg of wood. The input composition, for which Ni is the only variable, is provided in Table 1. The fixed conditions for the calculations are the pressure (1 bar) and the nature of the gasification agent ($CO_2$). The procedure consists of calculating the equilibrium every 10 °C, from 450 to 950 °C. At each calculation step, a constant amount $\langle A \rangle$ of $CO_2$ (in mol·kgw$^{-1}$) is added in the system, and the equilibrium composition is recorded. After each computation step, the gas phase is removed from the system to simulate an open system in which the gaseous species are not in contact with the condensed phases (Figure 1). Five additional steps are computed at 950 °C, to simulate the temperature plateau.

*2.2.3. Determination of $\langle A \rangle$.* During $CO_2$ gasification of char, the main reaction is the oxidation of carbon according to the so-called Boudouard reaction:

$$C(s) + CO_2(g) = 2CO(g)$$

When C(s) has fully reacted, the exhaust gas is thus mainly composed of unreacted $CO_2$(g). As illustrated in Figure 2, the amount of $CO_2$ which is added in the system at each calculation step ($\langle A \rangle$) plays an important role on the temperature at which total carbon cunsumption occurs.

In our simulations, $\langle A \rangle$ is adjusted so that the total consumption of carbon occurs at the same temperature as in the experimental reactor. Adjusting $\langle A \rangle$ is thus a simple way of introducing a kinetic restriction on the main gasification reaction. It can be noted from Figure 2 that if the temperature step is different from 10 °C, the $\langle A \rangle$ value will be modified

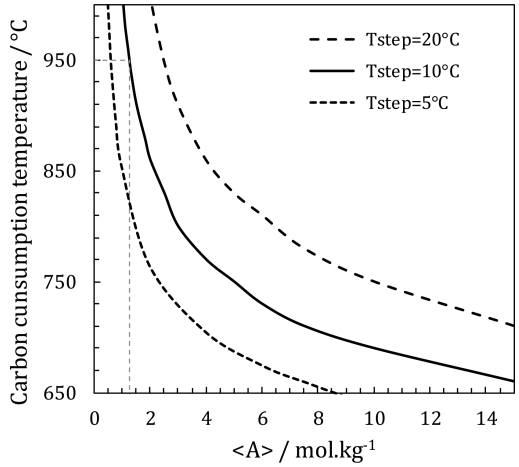


**Figure 2.** Evolution of the temperature of full carbon conversion with the amount v of $CO_2$ added at each calculation step.

proportionally: $\langle A \rangle$ is divided by 2 for a temperature step of 5 °C, and multiplied by 2 for a temperature step of 20 °C. This is consistent with the Boudouard equilibrium, because the carbon consumption at a given temperature is only depending on the $CO_2$ partial pressure.

The measured variation of CO(g) and $CO_2$(g) concentration in the exhaust gases is plotted in Figure 3. The total conversion

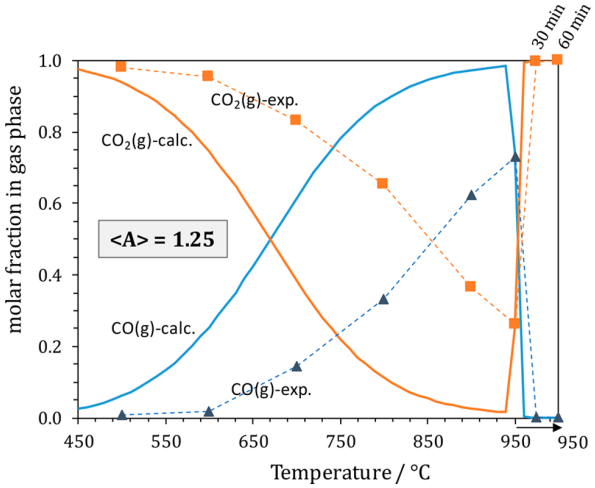


**Figure 3.** Comparison of the temperature evolution of $CO_2$ and CO molar fraction in the gas phase (i) measured in fixed bed reactor with raw wood (symbols and dashed lines) and (ii) calculated with $\langle A \rangle$ = 1.25 mol·kgw$^{-1}$ (continues lines).

of carbon occurs when the temperature reaches 950 °C. $\langle A \rangle$ was thus set to 1.25 mol·kgw$^{-1}$ (Figure 2), which is smaller than the experimental amount of $CO_2$ (1.78 mol·kgw$^{-1}$) flushed through the reactor during the 2 min necessary to raise the temperature by 10 °C, indicating that, on average, about 30% of the $CO_2$ does not take part in the gasification reaction.

It can be noted that for another reactor or operating conditions, the same methodology could be applied. $\langle A \rangle$ would then be obtained from experimental measurements of $CO_2$ and CO concentration profiles in the exhaust gases. These data are easy to obtain for any reactor with standard chromatography techniques.

The discrepancy between calculated and measured gas composition is large (temperature shift up to 200 °C), and is the direct consequence of kinetics control of gasification reactions. However, the main tendency (i.e., a large increase of CO proportion, followed by a significant drop after total carbon consumption) is represented with such calculation procedure, using one single parameter, which is not the case with closed system calculations.[27]

## 3. RESULTS AND DISCUSSION

**3.1. Catalytic Effect of Ni.** *3.1.1. Thermogravimetric Analyses.* Figure 4 shows the thermal analyses of the wood

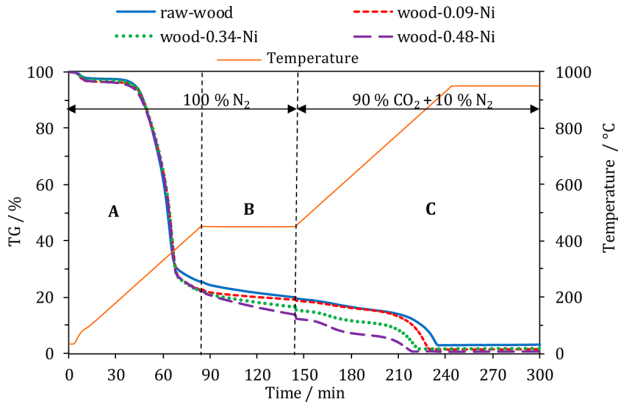


**Figure 4.** TG profiles of willow wood samples during pyro-gasification.

samples, which is divided into three main zones: the first temperature increases from 30 to 450 °C (A), the plateau at 450 °C for 1 h (B), and the second temperature raise to 950 °C, with a $CO_2$ flush (C). The pyrolysis step (A and B) was carried out under $N_2$, and the gasification step (C) under 90% $CO_2$ and 10% of $N_2$.

In Zone A, after a slight mass loss at about 100 °C corresponding to the water evaporation, a major mass loss occurs between 200 and 450 °C. As already finely described in the literature, this step corresponds to the hemicellulose and cellulose pyrolysis.[32]

In Zone B, the mass loss at the end of the isotherm increases by 6% for the wood-0.34-Ni and by 8% for the wood-0.48-Ni samples compared to that for raw wood. This feature is a clear indication of the influence of Ni on the pyrolysis step.

The gasification step (zone C) starts with the input of $CO_2$ at $t$ = 144 min. The differential of the TG signal (DTG) is presented in Figure 5 for zone C. For the impregnated samples wood-0.34-Ni and wood-0.48-Ni, an additional reaction is evidenced in the temperature range 470−660 °C. The DTG signal is more intense at high Ni concentrations. Furthermore, the main gasification reaction, which reaches a maximum rate at around 910 °C on raw wood, is shifted to lower temperatures with increasing amount of impregnated Ni (respectively 880, 845, and 820 °C for wood-0.09-Ni, wood-0.34-Ni, and wood-0.48-Ni). Figure 5 also shows that the increase of the Ni content in the samples enhances the gasification rate and, as a consequence, the variation of the gasification reaction kinetics.

These results are in-line with previous findings dealing with $CO_2$ gasification kinetics. Indeed, Figueiredo et al.[33] showed that the reactivity of impregnated carbon increases with the amount of Ni catalyst, with a decrease of the activation energy from 260 kJ·mol$^{-1}$ without Ni to about 110 J·mol$^{-1}$ for the Ni-

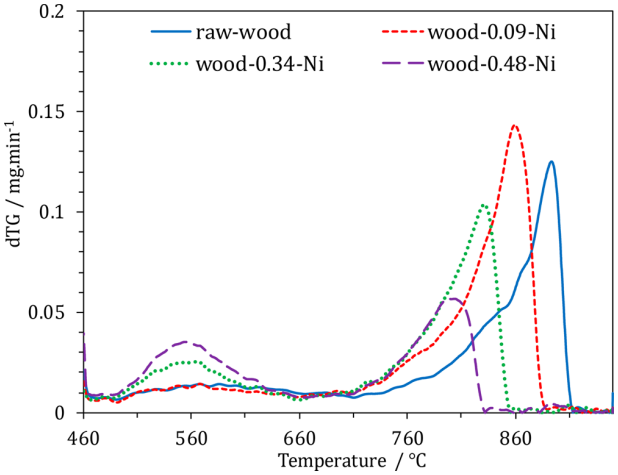


**Figure 5.** DTG profiles of willow wood samples during gasification. Inlet gas flow is composed of 5.4 L·h$^{-1}$ of $CO_2$ + 0.6 L·h$^{-1}$ of $N_2$.

catalyzed gasification reaction. Many other studies led to the conclusion that the kinetic parameters of the gas−solid reactions during $CO_2$ gasification are deeply affected by the presence and the amount of inorganic elements (either alkaline/alkaline-earth metals[34] or transition metals[19,33]). Di Blasi[35] stated that the char reactivity depends on three main characteristics: its porosity, its chemical structure, and the quantity of inorganic constituents. As evidenced in previous studies,[17,34] all those characteristics change when the wood or the char contains a high amount of a metal element.

The effect of Ni on the pyrolysis and gasification products is further discussed in the following sections on the basis of the data collected with the fixed-bed reactor.

*3.1.2. Fixed Bed Reactor Experiments Analysis.* The same experimental protocol (described in section 2.1.2) for the TG analysis is used for the bed reactor experiments.

*3.1.2.a. Pyrolysis Step in Fixed Bed Reactor.* The mass balance of the pyrolysis products, taking account gases, char, and tars, is presented in Table 2. Around 18−20% of the initial

**Table 2. Mass Balance of the Products Obtained from the Willow Wood Samples Pyrolysis in a Fixed-Bed Reactor Where *T* Ranges from Ambient to 450 °C in an Inlet Gas Flow of 6 L·h$^{-1}$ ($N_2$).**

| | gas yield/ wt % | char yield/ wt % | tar yield/ wt % | total/wt % |
|---|---|---|---|---|
| raw-wood | 14.1 ± 0.4 | 30.4 ± 0.4 | 36.6 ± 2.1 | 81.1 ± 2.9 |
| wood-0.09-Ni | 14.5 ± 0.6 | 29.7 ± 0.6 | 37.9 ± 1.4 | 82.1 ± 2.6 |
| wood-0.34-Ni | 15.0 ± 0.2 | 29.6 ± 0.9 | 36.2 ± 2.4 | 80.8 ± 3.5 |
| wood-0.48-Ni | 17.2 ± 0.1 | 28.9 ± 1.0 | 34.0 ± 2.6 | 80.1 ± 3.7 |

mass is missing. This is attributed to the condensation of tars on the reactor walls and in the gas circuit. Tars recovery is indeed a major and recurrent experimental difficulty, which requires the development of specific devices that were not available in our configuration. Nevertheless, the impact of Ni is rather clear from our experimental data: it leads to an increase of the total amount of gas and a decrease of the final amount of char.

The organic elemental composition and the ash content of the four samples of chars produced at 450 °C-60 min are presented in Table S1. The data show that both carbon and hydrogen contents in the chars decrease with the rise of the Ni content, in favor of the ash content. The highest variation is observed for hydrogen, with a decrease of 30% in the wood-0.48-Ni sample compared to that in the raw char.

This variation of the elemental composition of the chars agrees well with the amount and composition of gases produced during pyrolysis. The comparison of the impact of Ni impregnation on the total amount of $H_2$ and CO (in moles of gas formed per kg of wood) is presented in Figure 6. Additional data concerning $CO_2$, $CH_4$, $C_2H_4$, and $C_2H_6$ yields are plotted in Figure S1. The gas composition analysis shows a strong increase of the $H_2$ yield (multiplied by 6 and 14 times for wood-0.09-Ni and wood-0.48-Ni, respectively) and, to a lesser extent, of the CO formation (about 5% for the wood-0.48-Ni sample).

Given all these results, we can conclude that Ni impregnation in willow wood leads to significant changes during the pyrolysis step: (i) an increase of the total amount of gas produced and of the $H_2$ content in this gas and (ii) a drop of the char amount and of the H content in this char.

These phenomena are explained by a catalytic effect of Ni on biomass pyrolysis reactions (and more specifically on tars cracking inside the wood), as already well documented in the literature. For instance, Bru et al.[16] and Collard et al.[15] studied respectively the influence of Ni on the pyrolysis reactions of beech wood at 700 °C and oak wood at 600 °C. They both found a significant decrease in tar production in favor of gases, which is consistent with our results. Furthermore, Richardson et al.[17] showed that nickel metal nanoparticles act as a catalytic active phase for enhancing $H_2$ production during biomass pyrolysis. They also demonstrate that Ni is an active catalyst exclusively in its metal form related to a reduction reaction occurring between 450 and 600 °C.

In these studies, Ni concentrations ranged from 0.07 to 0.65 mol·kgw$^{-1}$ and pyrolysis temperatures from 600 to 700 °C. In our study, we show that the catalytic effect of Ni on pyrolysis reactions is effective at lower temperature (450 °C) with Ni contents as low as 0.016 mol·kgw$^{-1}$.

*3.1.2.b. Gasification in Fixed Bed Reactor.* Due to the low amounts of tars and ashes, as well as the difficulty to recover them, the mass balance of the gasification part of the experiment (ramp 450−950 °C + isotherm at 950 °C with $CO_2$ flush) was not established.

The total production of $H_2$ and CO is presented in Figure 7. The nickel content has no significant impact on the overall CO yield. However, the catalytic effect of Ni is noticeable on the $H_2$ yield with an increase of 1% and 22% for the wood-0.09-Ni and wood-0.48-Ni samples, respectively.

It is well attested that the $CO_2$ gasification of char leads to the formation of CO by the Boudouard reaction and results in low values of $H_2$/CO ratio.[36] In the present study, the $H_2$/CO ratio is around 0.05, with a content of $CO_2$ in the gas injected into the reactor equal to 88%. This is rather consistent with the data compiled by Butterman et al.,[37] which mention a $H_2$/CO ratio in the range 0.1−1.0 for $CO_2$ contents varying from 30 to 50% in the inlet gas, and a clear decrease of this ratio with increasing $CO_2$ content. Furthermore, the increase of the Ni content in the sample raises the $H_2$/CO value by 23% compared to that of raw wood.

The production profiles of $H_2$ and CO as a function of the temperature presented in Figure 8 provide more insights into the influence of the Ni content. Data for $CH_4$ are provided in Figure S2. Significant changes related to Ni are evidenced on

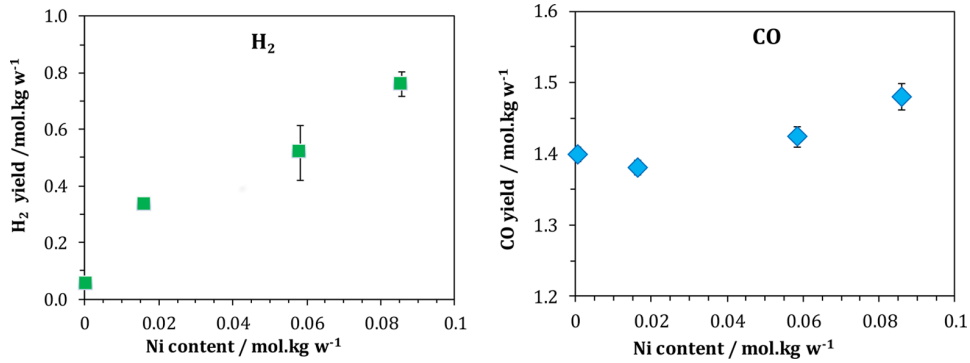


**Figure 6.** Influence of Ni content on the total production of $H_2$ and CO during pyrolysis of willow wood samples in a fixed-bed reactor where *T* ranges from ambient to 450 °C using an inlet gas flow of 6 $L{\cdot}h^{-1}$ ($N_2$).

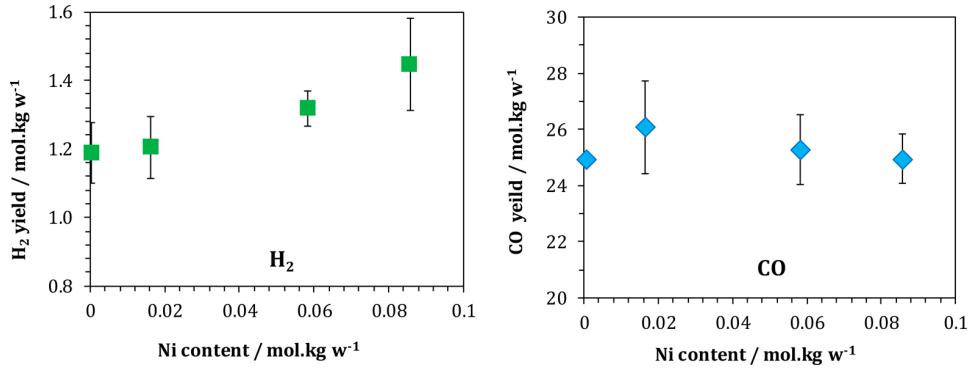


**Figure 7.** Influence of Ni content on the total production of $H_2$ and CO during gasification of willow wood samples in a fixed-bed reactor where *T* ranges from 450 to 950 °C while the inlet gas flow is 5.4 $L{\cdot}h^{-1}$ of $CO_2$ + 0.6 $L{\cdot}h^{-1}$ of $N_2$.

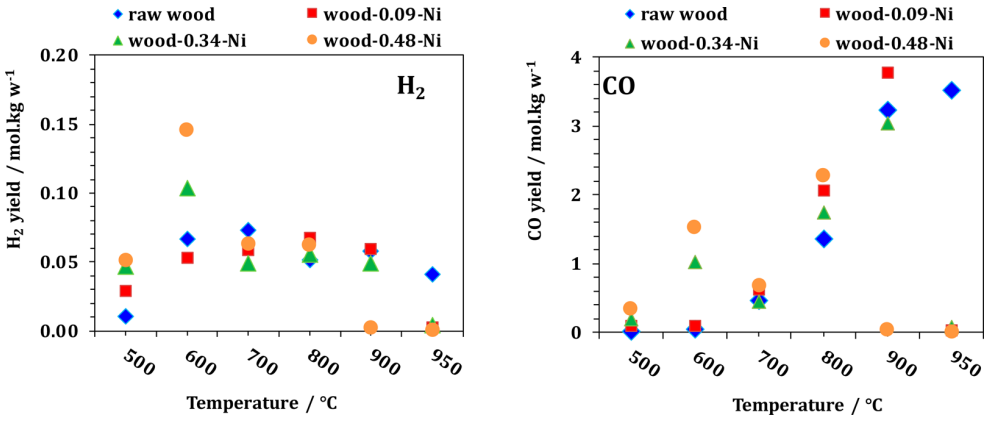


**Figure 8.** Influence of temperature on the amount of $H_2$ and CO produced during gasification of willow wood samples in a fixed-bed reactor using an inlet gas flow of 5.4 $L{\cdot}h^{-1}$ $CO_2$ + 0.6 $L{\cdot}h^{-1}$ $N_2$.[25]

these profiles, essentially between 500 and 800 °C. The $H_2$ yield increases by 55−118% at 600 °C for wood-0.34-Ni and wood-048-Ni compared to that of raw wood, and $H_2$ production stops at lower temperature in the presence of Ni. Similarly, the CO yield increases up to 1 and 1.5 $mol{\cdot}kgw^{-1}$ at 600 °C for wood-0.34-Ni and wood-0.48-Ni samples, respectively, whereas it is negligible at low Ni content. The CO production reaches a maximum at 900 °C for the wood-0.34-Ni sample and at 800 °C for the wood-0.48-Ni sample. For the wood-0.09-Ni and raw wood, the maximum of CO production is detected at 900 and 950 °C respectively.

Combined with TGA analysis, the data collected from the fixed-bed reactor experiments provide a rather clear picture of the catalytic influence of Ni on gasification. Indeed, for Ni contents higher than 0.09 $mol{\cdot}kgw^{-1}$, an additional reaction occurs between 500 and 600 °C. This reaction results in a significant mass loss of the char and produces noticeable amounts of $H_2$(g) and CO(g). Furthermore, the presence of nickel in the samples decreases the temperature onset of the main gasification reaction, from 920 °C in raw wood down to 830 °C with wood-0.48-Ni.

The catalytic effect of nickel on both pyrolysis and gasification is thus clearly evidenced and characterized by quantification of the major reaction products (char, tars, $H_2$, CO) during the process. Furthermore, this catalytic effect depends on the initial quantity of nickel.

**3.2. Ni Speciation.** *3.2.1. Speciation by XRD Characterizations.* The XRD (X-ray diffraction) analyses of the char samples obtained by pyrolysis at 450 °C are presented in Figure 9. The diffraction patterns of the four samples show the

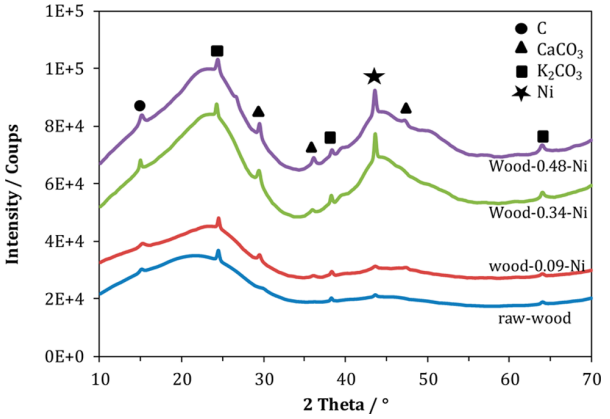


**Figure 9.** XRD analyses of the char samples produced at 450 °C-60 min.

presence of a dominant amorphous phase. The presence of graphite carbon, calcium carbonate, and potassium carbonate is detected in all samples. A crystalline phase corresponding to Ni metal (with fcc structure) is also evidenced in wood-0.34-Ni and wood-0.48-Ni samples, but it is not detectable in the wood-0.09-Ni sample.

Furthermore, the diffractogram of the residue obtained at 800 °C also show the presence of nickel in its metal form (Figure 10).

The X-ray diffractograms of the ashes recovered at the end of the pyro-gasification reaction are presented in Figure 11. They indicate the presence of nickel oxide (NiO) in the three impregnated samples, which shows that Ni metal undergoes oxidation at some point during the process.

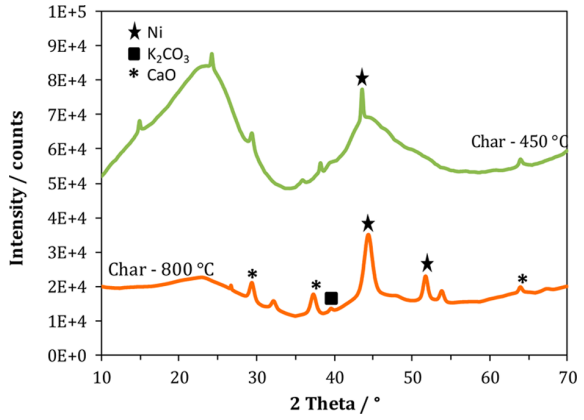


**Figure 10.** XRD analyses of the chars produced at 450 °C-60 min and 800 °C for the wood-0.34-Ni sample.

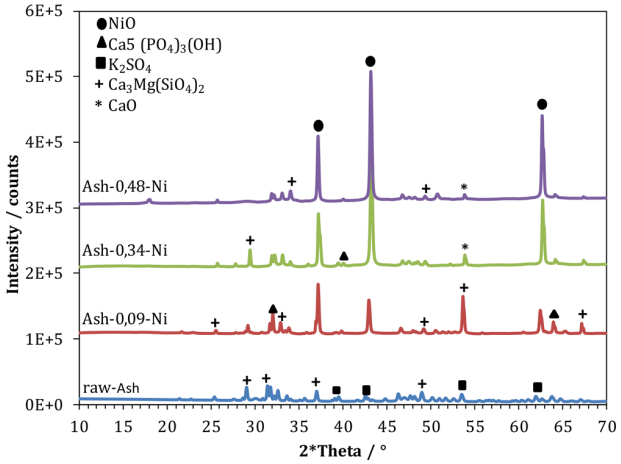


**Figure 11.** XRD analyses of the ashes samples produced at 950 °C-60 min.

*3.2.2. Speciation by Thermodynamic Calculations.* The calculated temperature evolution of the chemical speciation of nickel for three samples is presented in Figure 12. The Ni speciation results for the wood-0.48-Ni sample are similar to those found for the wood-0.34-Ni sample. For this reason, the speciation results of the wood-0.48-Ni sample are not included in Figure 12.

A first comment is that, independently of its initial quantity, Ni fully remains in condensed phases, either in solids or in the slag solution phase.

In any case, Ni forms intermetallic compounds with Sb (NiSb) and Sn ($Ni_3Sn_x$, with $1 \leq x \leq 3$), which are the most stable compounds that bind to Ni among the 26 elements considered in the biomass. A consequence is that, for raw wood (for which the Sb and Sn content is higher than the Ni content), there is no free Ni metal on the entire temperature range.

When more Ni is available in the system (wood-0.09-Ni), a second type of compound forms ($Ni_3S_2$), which is stable up to about 700 °C.

With higher Ni contents (wood-0.34-Ni and wood-0.48-Ni), Ni is predominantly present in its metal form through the whole temperature range.

At the end of the pyro-gasification reaction, when all carbon is consumed, nickel progressively oxidizes into NiO, as illustrated in Figure 12. According to the model, part of the oxide dissolves in the liquid slag phase. Figure 13 gives an additional insight into the behavior of Ni in the pyro-gasification reactor. Indeed, in the 450–950 °C temperature range, the equilibrium oxygen partial pressure ($PO_2$) resulting of the equilibrium between $CO_2$ and wood is lower than the equilibrium $PO_2$ between Ni and NiO. This means that the stable form of nickel is the metal form. However, when all carbon has been consumed, the atmosphere switches to pure $CO_2$(g), with a higher oxygen potential that leads to oxidation of Ni into NiO.

*3.2.3. Discussion.* The combination of XRD characterization and thermodynamic calculations provides a concordant picture on the behavior of Ni during the pyro-gasification. Indeed, nickel is detected in its metal form in solid residues recovered at 450 and 800 °C, provided that Ni quantity is sufficient for detection. The final ashes contain predominantly nickel oxide, due to its oxidation at the end of the process.

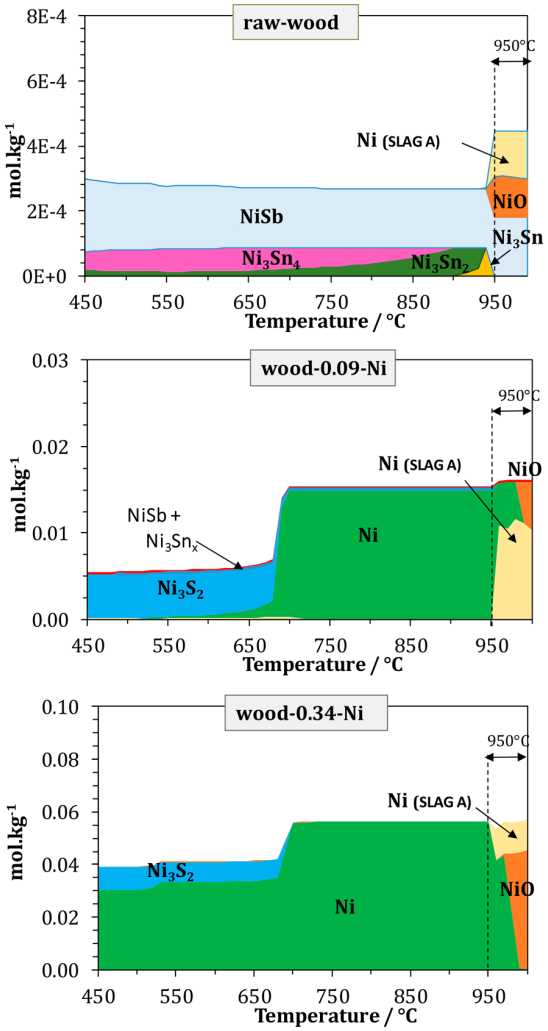


**Figure 12.** Calculated Ni speciation as function of Ni content, for $T$ = 450–950 °C. Additional calculation steps for $T$ = 950 °C are represented on the right extremity of the $x$-axis.

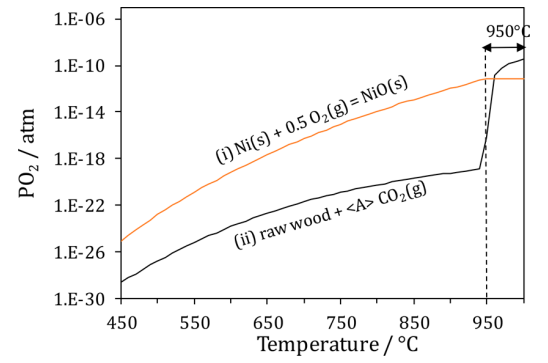


**Figure 13.** Influence of temperature on oxygen partial pressure ($PO_2$) at equilibrium: (i) Ni-NiO equilibrium; (ii) raw wood.

As already mentioned, Ni must be in its metal form to cause a catalytic effect on the pyro-gasification reactions. The thermodynamic speciation indicates that, at low temperature, sulfur has a high affinity with Ni. As reported in several experimental studies carried out on various Ni-based catalysts,[32,33] sulfur can be an important inhibitor of its catalytic activity. Therefore, a threshold content of Ni is required in the biomass to observe the catalytic effect of Ni. Below this threshold value, Ni is trapped in sulfide compounds. Furthermore, it is expected that at temperature higher than 700 °C, the decomposition of nickel sulfide enhances the catalytic effect of Ni.

### 3.3. Ni Effect on the Behavior of Inorganic Elements.

*3.3.1. Influence of Ni on Ashes Composition.* The elemental composition of ashes (measured and calculated with FactSage) is presented in Figure 14. The chemical analyses performed by ICP-OES indicate that the ashes are mainly composed of Ca, K, Mg, P, S, and Si, plus a growing proportion of Ni for impregnated samples. This is consistent with the major phases identified by XRD (Figure 12): $Ca_5(PO_4)_3(OH)$, $K_2SO_4$, $Ca_3Mg(SiO_4)_2$, and CaO, plus NiO. The calculated elemental composition of the ashes, determined as the sum of all solid compounds at 950 °C, reproduces remarkably well the experimental data.

Apart from S, whose behavior will be further discussed in the next section, both calculated and measured data show that there is no major influence of the initial Ni amount on the content of the main elements of the ashes.

As discussed in our previous work,[27] the adopted calculation procedure leads to a satisfactory reproduction of trace elements contents measured in raw wood ashes recovered after $CO_2$ gasification. The wood samples impregnated with Ni studied in the present work did not lead to major changes in the behavior of trace elements either. Some of them were shown to fully or partially volatilize: S, Cd, Pb, Zn, Cl, Sn, K, Na and F.

*3.3.2. Influence of Ni on Sulfur Behavior.* As discussed in details by Kaknics et al.,[38] sulfur has been shown to volatilize to a large extent during pyro-gasification at low temperature, in the form of $H_2S(g)$ and $COS(g)$, when placed in the reducing environment constituted by $C(s)$ and $CO_2(g)$. Our experimental data confirm that, for raw wood, more than 50% of the initial sulfur is not found in the final solid residue. Furthermore, the amount of sulfur in the ashes increases significantly with the Ni content. These results are consistent with the calculated amount of S in gas phase presented in Figure 15. Indeed, Ni promotes the trapping of sulfur in a $Ni_3S_2$ solid phase up to about 650 °C. At higher temperatures, S is then trapped in a CaS solid phase. When the initial nickel content is significantly higher than the sulfur content, most of sulfur is thus trapped in the solid residue. This behavior is rather similar to the observations from Mortensen[39] and Woolcock[40] in the case of nickel catalysts for methane re-forming. The authors observed sulfur trapping on nickel, resulting in the catalyst's poisoning.

## 4. CONCLUSIONS

The combination of experimental and thermodynamic approaches helped to evaluate the role and the behavior of Ni during the pyro-gasification reaction of impregnated willow samples in a $CO_2$ atmosphere. The experimental tests allowed us to quantify the solid and gaseous products during pyro-gasification. The thermodynamic simulation methodology consisted of (i) considering an open system to simulate a gas flow in the system and (ii) determining the amount of gasification agent added at each calculation step with experimental measurements of $CO_2$ and CO concentration profiles, these data being easy to obtain for any reactor with standard chromatography techniques. The thermodynamic simulations were consistent with most of the experimental

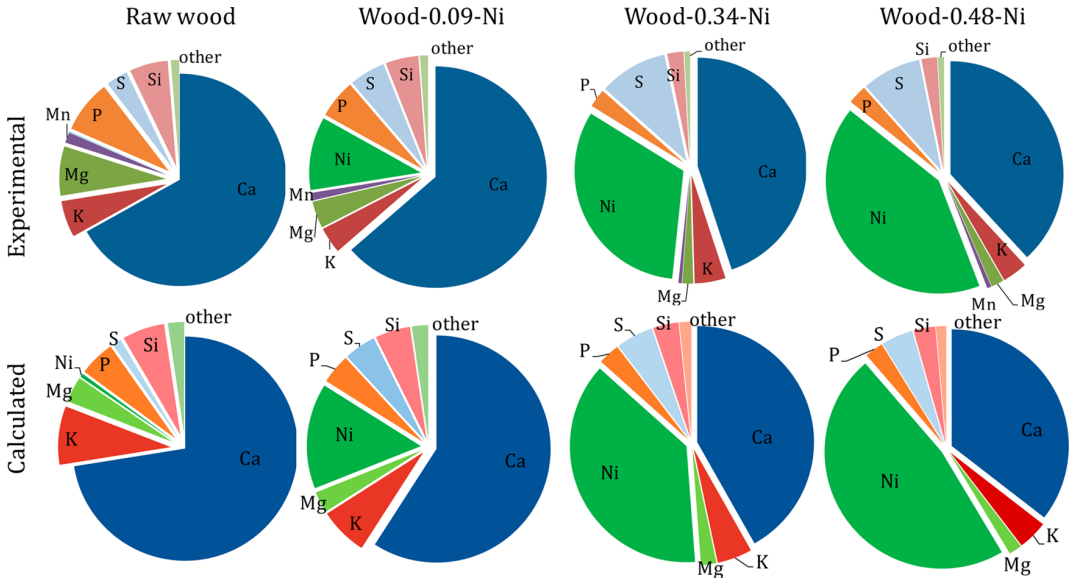


**Figure 14.** Comparison between experimental and calculated ashes elemental composition.

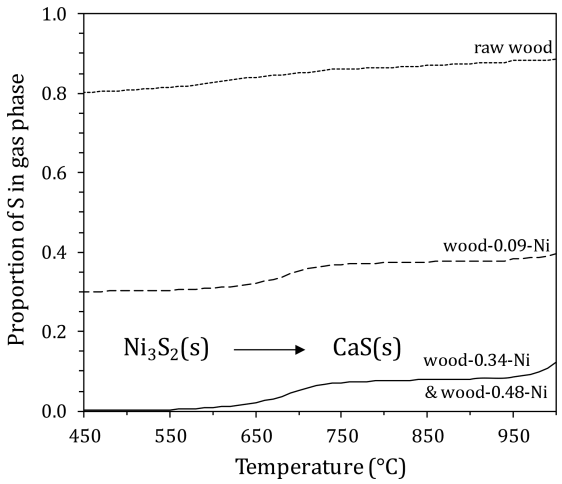


**Figure 15.** Calculated influence of temperature and Ni content on the proportion of sulfur in the gaseous phase.

data (chemical analysis of ashes, XRD of the solid residues at 450, 800, and 950 °C), even if the exact amount of Ni linked with a catalytic activity could not be determined with accuracy.

Based on this methodological approach, the main results of the study are

- Ni has a noticeable catalytic activity even at low content (between 0.016 and 0.086 mol·kgw$^{-1}$)
- Ni stays in an active metal form as long as some carbon is left in the reactor due to the low oxygen potential of the system C + $CO_2$
- Ni prevents the evaporation of sulfur during the gasification, due to the formation of a stable $Ni_3S_2$(s) phase

Our methodological contribution constitutes a powerful approach that would allow for future investigation of the influence of other metals such as Cu and Fe during pyro-gasification reactions, as well as detecting potential synergies between inorganic elements such as the Ni−S interactions evidenced in this work .

## ■ ASSOCIATED CONTENT

### Supporting Information

The Supporting Information is available free of charge on the ACS Publications website at DOI: 10.1021/acs.iecr.7b05201.

Table S1, elementary composition of the chars; Figure S1, influence of Ni content on the total production of $C_nH_m$ and $CO_2$ during pyrolysis; Figure S2, influence of temperature on the amount of $CH_4$ produced during gasification (PDF)

## ■ AUTHOR INFORMATION


### Corresponding Author

*L. Cassayre. E-mail address: laurent.cassayre@ensiacet.fr

### ORCID

Laurent Cassayre: 0000-0001-6876-6086


### Notes

The authors declare no competing financial interest.

## ■ REFERENCES


(1) Radmanesh, R.; Courbariaux, Y.; Chaouki, J.; Guy, C. A Unified Lumped Approach in Kinetic Modeling of Biomass Pyrolysis. *Fuel* **2006**, *85*, 1211−1220.

(2) Gupta, A. K.; Sinha, S. Phytoextraction Capacity of the Plants Growing on Tannery Sludge Dumping Sites. *Bioresour. Technol.* **2007**, *98*, 1788−1794.

(3) Lievens, C.; Carleer, R.; Cornelissen, T.; Yperman, J. Fast Pyrolysis of Heavy Metal Contaminated Willow: Influence of the Plant Part. *Fuel* **2009**, *88*, 1417−1425.

(4) Zhang, X.; Laubie, B.; Houzelot, V.; Plasari, E.; Echevarria, G.; Simonnot, M.-O. Increasing Purity of Ammonium Nickel Sulfate Hexahydrate and Production Sustainability in a Nickel Phytomining Process. *Chem. Eng. Res. Des.* **2016**, *106*, 26−32.

(5) Houzelot, V.; Laubie, B.; Pontvianne, S.; Simonnot, M.-O. Effect of up-Scaling on the Quality of Ashes Obtained from Hyper-accumulator Biomass to Recover Ni by Agromining. *Chem. Eng. Res. Des.* **2017**, *120*, 26−33.

(6) Wu, S.; Xu, Y.; Sun, J.; Cao, Z.; Zhou, J.; Pan, Y.; Qian, G. Inhibiting Evaporation of Heavy Metal by Controlling Its Chemical Speciation in MSWI Fly Ash. *Fuel* **2015**, *158*, 764−769.
(7) Toledo, J. M.; Corella, J.; Corella, L. M. The Partitioning of Heavy Metals in Incineration of Sludges and Waste in a Bubbling Fluidized Bed. 2. Interpretation of Results with a Conceptual Model. *J. Hazard. Mater.* **2005**, *126*, 158−168.
(8) Šyc, M.; Pohořelý, M.; Jeremiáš, M.; Vosecký, M.; Kameníková, P.; Skoblia, S.; Svoboda, K.; Punčochář, M. Behavior of Heavy Metals in Steam Fluidized Bed Gasification of Contaminated Biomass. *Energy Fuels* **2011**, *25*, 2284−2291.
(9) Yuan, C.-S.; Lin, H.-Y.; Wu, C.-H.; Liu, M.-H. Partition and Size Distribution of Heavy Metals in the Flue Gas from Municipal Solid Waste Incinerators in Taiwan. *Chemosphere* **2005**, *59*, 135−145.
(10) Nzihou, A.; Stanmore, B. The Fate of Heavy Metals during Combustion and Gasification of Contaminated Biomass-a Brief Review. *J. Hazard. Mater.* **2013**, *256*−*257*, 56−66.
(11) Sutton, D.; Kelleher, B.; Ross, J. R. H. Review of Literature on Catalysts for Biomass Gasification. *Fuel Process. Technol.* **2001**, *73*, 155−173.
(12) Lahijani, P.; Zainal, Z. A.; Mohamed, A. R.; Mohammadi, M. $CO_2$ Gasification Reactivity of Biomass Char: Catalytic Influence of Alkali, Alkaline Earth and Transition Metal Salts. *Bioresour. Technol.* **2013**, *144*, 288−295.
(13) Huo, W.; Zhou, Z.; Chen, X.; Dai, Z.; Yu, G. Study on $CO_2$ Gasification Reactivity and Physical Characteristics of Biomass, Petroleum Coke and Coal Chars. *Bioresour. Technol.* **2014**, *159*, 143−149.
(14) Šyc, M.; Pohořelý, M.; Kameníková, P.; Habart, J.; Svoboda, K.; Punčochář, M. Willow Trees from Heavy Metals Phytoextraction as Energy Crops. *Biomass Bioenergy* **2012**, *37*, 106−113.
(15) Collard, F.-X.; Blin, J.; Bensakhria, A.; Valette, J. Influence of Impregnated Metal on the Pyrolysis Conversion of Biomass Constituents. *J. Anal. Appl. Pyrolysis* **2012**, *95*, 213−226.
(16) Bru, K.; Blin, J.; Julbe, A.; Volle, G. Pyrolysis of Metal Impregnated Biomass: An Innovative Catalytic Way to Produce Gas Fuel. *J. Anal. Appl. Pyrolysis* **2007**, *78*, 291−300.
(17) Richardson, Y.; Blin, J.; Volle, G.; Motuzas, J.; Julbe, A. In Situ Generation of Ni Metal Nanoparticles as Catalyst for $H_2$-Rich Syngas Production from Biomass Gasification. *Appl. Catal., A* **2010**, *382*, 220−230.
(18) Huang, Y.; Yin, X.; Wu, C.; Wang, C.; Xie, J.; Zhou, Z.; Ma, L.; Li, H. Effects of Metal Catalysts on $CO_2$ Gasification Reactivity of Biomass Char. *Biotechnol. Adv.* **2009**, *27*, 568−572.
(19) Lahijani, P.; Zainal, Z. A.; Mohamed, A. R. Catalytic Effect of Iron Species on $CO_2$ Gasification Reactivity of Oil Palm Shell Char. *Thermochim. Acta* **2012**, *546*, 24−31.
(20) Ma, C.; Backman, R.; Öhman, M. Thermochemical Equilibrium Study of Slag Formation during Pressurized Entrained-Flow Gasification of Woody Biomass. *Energy Fuels* **2015**, *29*, 4399−4406.
(21) Konttinen, J.; Backman, R.; Hupa, M.; Moilanen, A.; Kurkela, E. Trace Element Behavior in the Fluidized Bed Gasification of Solid Recovered Fuels − A Thermodynamic Study. *Fuel* **2013**, *106*, 621−631.
(22) Koukkari, P.; Penttilä, K.; Hack, K.; Petersen, S. CHEMSHEET − An Efficient Worksheet Tool for Thermodynamic Process Simulation. In *Microstructures, Mechanical Properties and Processes - Computer Simulation and Modelling*; Bréchet, Y., Ed.; Wiley-VCH: Weinheim, 2000; Vol. 3, pp 323−330.
(23) Kangas, P.; Koukkari, P.; Hupa, M. Modeling Biomass Conversion during Char Gasification, Pyrolysis, and Torrefaction by Applying Constrained Local Thermodynamic Equilibrium. *Energy Fuels* **2014**, *28*, 6361−6370.
(24) Yung, M. M.; Jablonski, W. S.; Magrini-Bair, K. A. Review of Catalytic Conditioning of Biomass-Derived Syngas. *Energy Fuels* **2009**, *23* (4), 1874−1887.
(25) Said, M.; Cassayre, L.; Dirion, J.-L.; Joulia, X.; Nzihou, A. Effect of Nickel Impregnation on Wood Gasification Mechanism. *Waste Biomass Valorization* **2017**, *8*, 2843−2852.
(26) Said, M.; Cassayre, L.; Dirion, J.-L.; Nzihou, A.; Joulia, X. Behavior of Heavy Metals during Gasification of Phytoextraction Plants: Thermochemical Modelling. *Comput.-Aided Chem. Eng.* **2015**, *37*, 341−346.
(27) Said, M.; Cassayre, L.; Dirion, J.-L.; Joulia, X.; Nzihou, A. On the Relevance of Thermodynamics to Predict the Behaviour of Inorganics during $CO_2$. *Comput.-Aided Chem. Eng.* **2017**, *40*, 2671−2676.
(28) Degroot, W. F.; Shafizadeh, F. The Influence of Exchangeable Cations on the Carbonization of Biomass. *J. Anal. Appl. Pyrolysis* **1984**, *6*, 217−232.
(29) Mahar, A.; Wang, P.; Ali, A.; Awasthi, M. K.; Lahori, A. H.; Wang, Q.; Li, R.; Zhang, Z. Challenges and Opportunities in the Phytoremediation of Heavy Metals Contaminated Soils: A Review. *Ecotoxicol. Environ. Saf.* **2016**, *126*, 111−121.
(30) Bale, C. W.; Bélisle, E.; Chartrand, P.; Decterov, S.; Eriksson, G.; Hack, K.; Jung, I.-H.; Kang, Y.-B.; Melançon, J.; Pelton, A. D.; Robelin, C.; Peterson, S. FactSage Thermochemical Software and Databases — Recent Developments. *CALPHAD: Comput. Coupling Phase Diagrams Thermochem.* **2009**, *33*, 295−311.
(31) Lindberg, D.; Backman, R.; Chartrand, P.; Hupa, M. Towards a Comprehensive Thermodynamic Database for Ash-Forming Elements in Biomass and Waste Combustion — Current Situation and Future Developments. *Fuel Process. Technol.* **2013**, *105*, 129−141.
(32) Yang, H.; Yan, R.; Chen, H.; Lee, D. H.; Zheng, C. Characteristics of Hemicellulose, Cellulose and Lignin Pyrolysis. *Fuel* **2007**, *86*, 1781−1788.
(33) Figueiredo, J. L.; Rivera-Utrilla, J.; Ferro-Garcia, M. A. Gasification of Active Carbons of Different Texture Impregnated with Nickel, Cobalt and Iron. *Carbon* **1987**, *25*, 703−708.
(34) Duman, G.; Uddin, Md. A.; Yanik, J. The Effect of Char Properties on Gasification Reactivity. *Fuel Process. Technol.* **2014**, *118*, 75−81.
(35) Di Blasi, C. Combustion and Gasification Rates of Lignocellulosic Chars. *Prog. Energy Combust. Sci.* **2009**, *35*, 121−140.
(36) Jang, W.-J.; Jeong, D.-W.; Shim, J.-O.; Kim, H.-M.; Roh, H.-S.; Son, I. H.; Lee, S. J. Combined Steam and Carbon Dioxide Reforming of Methane and Side Reactions: Thermodynamic Equilibrium Analysis and Experimental Application. *Appl. Energy* **2016**, *173*, 80−91.
(37) Butterman, H. C.; Castaldi, M. J. $CO_2$ as a Carbon Neutral Fuel Source via Enhanced Biomass Gasification. *Environ. Sci. Technol.* **2009**, *43*, 9030−9037.
(38) Kaknics, J.; Defoort, F.; Poirier, J. Inorganic Phase Transformation in *Miscanthus* Ash. *Energy Fuels* **2015**, *29*, 6433−6442.
(39) Mortensen, P. M.; Dybkjær, I. Industrial Scale Experience on Steam Reforming of $CO_2$-Rich Gas. *Appl. Catal., A* **2015**, *495*, 141−151.
(40) Woolcock, P. J.; Brown, R. C. A Review of Cleaning Technologies for Biomass-Derived Syngas. *Biomass Bioenergy* **2013**, *52*, 54−84.